ACS Catalysis

Research Article

pubs.acs.org/acscatalysis

Sustainable Production of Acrylic Acid: Catalytic Performance of Hydroxyapatites for Gas-Phase Dehydration of Lactic Acid

Bo Yan, Li-Zhi Tao, Yu Liang, and Bo-Qing Xu*

Innovative Catalysis Program, Key Lab of Organic Optoelectronics & Molecular Engineering, Department of Chemistry, Tsinghua University, Beijing, 100084, China

Supporting Information

ABSTRACT: Hydroxyapatites (HAP_m-T) of varying molar Ca/P ratios m (1.58−1.69) and calcination temperatures T (360−700 °C) were prepared and comprehensively characterized by nitrogen adsorption, TG, XPS, XRD, CO_2-TPD, and NH_3-TPD and were employed to catalyze the gas-phase dehydration of lactic acid (LA) to produce acrylic acid (AA). While the texture and crystallinity of the HAP_m-T sample were affected little by variation of m, its surface acidity decreased but basicity increased with the increase in m. The HAP_m-T sample with a higher T showed a higher crystallinity but lower surface area, acidity, and basicity. The conversion of LA decreased with increasing either m or T of the HAP_m-T catalyst; the selectivity for AA maximized at m = 1.62 but decreased steadily with the T increase. The $HAP_{1.62}$-360 sample (m = 1.62, T = 360 °C) was identified as the most efficient catalyst, offering an AA yield as high as 50−62% for longer than 8 h (AA selectivity: 71−74 mol %) under optimized reaction conditions (360 °C, $WHSV_{LA}$= 1.4−2.1 h^{-1}). Correlating the catalyst performance with its surface acidity and basicity disclosed that the LA consumption rate increased linearly with the acidity/basicity ratio, but volcano-type dependence appeared between the AA production rate and the acidity/basicity ratio, which reveals a kind of cooperative acid−base catalysis for selective AA production. The HAP_m-T catalysts became more or less deactivated after reaction, but the reacted ones could be fully regenerated by in situ treatment with flowing air.

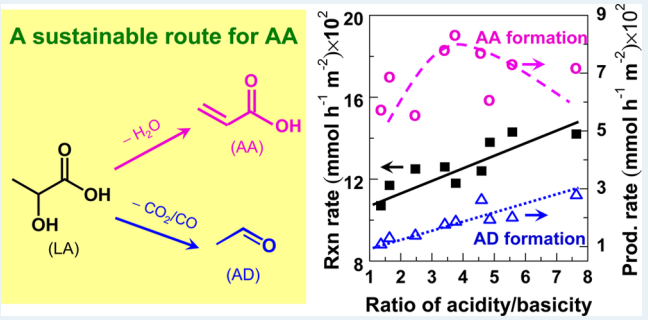

KEYWORDS: *hydroxyapatites, acid−base catalysis, lactic acid, acrylic acid, catalytic dehydration, sustainable chemistry*

1. INTRODUCTION

Increasing concern about the availability of fossil raw materials has led the chemical industries to search for alternative natural resources (bioresources) as the feedstock for chemicals and materials.[1,2] Among many possible feedstock candidate molecules that are derivable from bioresources is lactic acid (LA), a well-recognized biobased α-hydroxy acid.[3,4] Catalytic activation of its α-hydroxy and/or β-hydrogen with solid acid−base catalysts could enable a selective dehydration reaction of LA to produce acrylic acid (AA), an important intermediate for a number of key molecules and materials such as acrylate polymers.[5] Research activities to develop highly efficient acid−base catalysts for this LA-to-AA (LTA) chemistry in the gas-phase would lead a green and sustainable alternative to current commercial AA production technology based on a two-step selective catalytic oxidation process using petroleum (propylene) as the feedstock.[6,7]

The first report on the gas-phase LTA reaction was documented 50 years ago, using mixed metal phosphate and sulfate as catalysts; a mixed $Na_2SO_4/CaSO_4$ (molar ratio = 1:25) was identified to offer an AA yield of 68%.[8] This work stimulated an interest to search for various phosphate[9−16] and sulfate[11,17] based catalysts for the reaction. The possible gas-phase reactions of LA under varying conditions over supported phosphate salts and alkali-metal salts were documented by Miller et al.,[18−24] who showed that the catalytic LTA reaction was always accompanied by several competing reactions including decarbonylation or decarboxylation reactions[25] that produce acetaldehyde (AD, the main byproduct), a condensation reaction producing 2,3-pentanedione (2,3-PD), and a hydrogenolysis reaction (with hydrogen produced on-site during the reaction) producing propionic acid (PA) and 1-hydroxyacetone (1-HA),[18−24] as depicted in Scheme 1. The formation of lactide in the LTA reaction was clearly detected only in very recent works.[14,16] The reaction conditions in favor of a high selectivity toward the formation of AA (LTA) were a properly high temperature (ca. 350−370 °C), low LA partial pressure (0.1−0.4 MPa), and short contact time (0.3−0.5 s), while the reaction under the counter conditions (high LA partial pressure, 0.5 MPa; low temperature, 280−300 °C; and long residence time, 2−4 s) could instead favor the formation of 2,3-PD.[18,21] They also showed that LA conversion and yields for both AA and 2,3-PD increased but the yield for AD decreased with increasing the catalyst basicity (Na_3PO_4 >

Received: November 10, 2013
Revised: April 30, 2014
Published: May 1, 2014

Scheme 1. Gas-Phase Dehydration of Lactic Acid and Its Competing Reactions

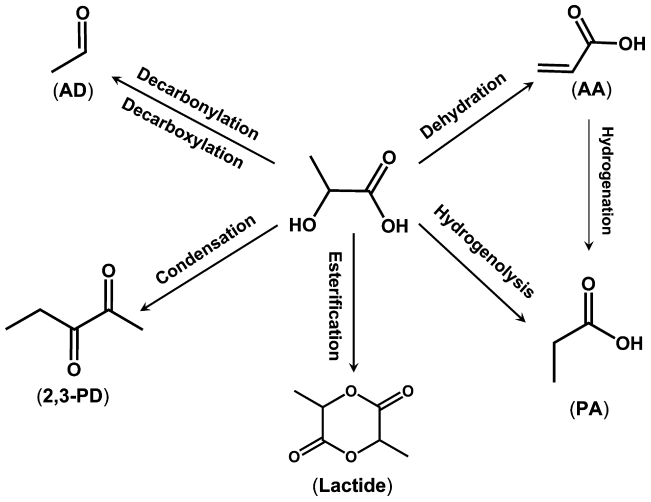

Na_2HPO_4 > NaH_2PO_4) and that the presence of alkali ions would prevent the formation of AD by generating on the working catalyst surface alkali lactate intermediate, which would protect the carboxyl group in LA from decarbonylation or decarboxylation.[25] However, the selectivity to AA was no higher than 50% in their works.[18−24] Recently, NaY zeolites modified with alkaline, alkaline earth, or rare earth metal ions (like K^+, Ca^{2+}, and La^{3+}) or their oxides were used as LTA catalysts in the work of Huang et al.[26−31] These modifications lowered the acidity but increased the basicity of the NaY samples, leading to higher selectivity for AA formation and lower selectivity for the formation of AD and surface carbon deposits. The highest selectivity for AA was reported to be 68 mol % over NaY zeolites modified by KI.[28] These previous works indicate that the gas-phase LTA reaction would require a copresence on the catalyst surface of weak acidity and weak basicity.[14−16] Strongly acidic sites were assumed to promote the competing decarboxylation/decarbonylation reaction leading AD formation[18,19,26−31] while on the other hand strongly basic sites could interact strongly with LA, resulting in formation of scattering unwanted and/or unknown products, including 2,3-PD and PA.[14−16]

As phosphates with apatite structure, hydroxyapatites (HAP) are known as important acid−base catalysts.[32−37] The stoichiometric formula of HAP is $Ca_{10}(PO_4)_6(OH)_2$ (molar Ca/P = 1.67), a deviation from this stoichiometry by varying the Ca/P ratio in the range of 1.50−1.67 would offer nonstoichiometric calcium phosphate samples with systematically tailored surface acid−base properties.[32,37] This strategy was previously used to study the acid−base catalysis for alcohol conversion.[32−37] The sample of Ca/P = 1.58 was found highly acidic and showed catalytic activity only for alcohol dehydration. On the other hand, the stoichiometric HAP sample (Ca/P = 1.67), which appeared less acidic but more basic, was found catalytically active for both the dehydration and dehydrogenation of alcohols. In this paper, a series of HAP_m-T samples with varying molar Ca/P ratios (m) and calcination temperatures (T) were prepared, characterized with different physicochemical techniques and used to catalyze the gas-phase LTA reaction. The $HAP_{1.62}$-360 sample is identified as the most effective for the selective formation of AA from LA, showing an AA selectivity as high as 71−74 mol % and AA yield of 50−62%. Attempts are made to correlate the catalytic performance of these HAP_m-T samples with their surface acidity and basicity, which disclose that both the acidic and basic sites are essential to the LTA catalysis.

2. EXPERIMENTAL SECTION

2.1. Catalyst Preparation. The HAP_m-T samples were prepared by varying a molar Ca/P ratio m between 1.58 and 1.69 and calcination temperature T between 360 and 700 °C, according to the method described previously.[37] Typically, 250 mL of aqueous solution of 0.250 M $(NH_4)_2HPO_4$ was added dropwise under stirring into 250 mL of aqueous $Ca(NO_3)_2$ solution containing the desired amount of $Ca(NO_3)_2$. The resultant suspensions were aged at 40 °C and pH = ca. 10 for 12 h before the product precipitates were collected by filtration. Precipitates were then washed extensively with deionized water until conductivity of the filtrate was less than 10 μS cm^{-1}, measured with a DDS-307W conductivity meter (LIDA Instrument, Shanghai). An overnight drying of the washed solid powders at 110 °C produced the precursor samples of HAP_m-T. These precursor samples were then calcined for 5 h at a temperature in the range of T = 360−700 °C in flowing air to make the final HAP_m-T sample. The molar Ca/P ratios in the calcined samples were m = 1.69, 1.68, 1.62, 1.60, and 1.58, as measured by X-ray fluorescence (XRF).

2.2. Characterizations. The overall composition of the HAP_m-T samples was determined by XRF analysis, conducted on a Shimadzu XRF-1800 fluorescence spectrometer coupled with a Rh radiation source at 40 kV and 70 mA and with scintillation counters and gas flow proportional counters as detectors. The samples were pressed into flat discs (20 mm diameter, 4−5 mm thickness) on a briquetting machine. PKα and CaKα spectra lines were used, respectively, for identification of Ca and P elements; their quantifications were done with the BG-FP method, from which the Ca/P ratio (m) was obtained.

X-ray diffraction (XRD) patterns were measured on a Bruker D8 Advance X-ray diffractometer with a Ni-filtered CuKα (λ = 0.15406 nm) radiation source at 40 kV and 40 mA and silicon array detectors. The samples were pressed into flat discs (Ø2 mm, thickness of 1 mm) in a homemade mold. The patterns were recorded for 2θ angles between 10° and 90° at a rate of 8°/min.

The surface area, pore volume, and average pore diameter data were obtained from nitrogen adsorption−desorption isotherms at 77 K. The elemental composition and chemical state of the samples were probed by X-ray photoelectron spectroscopy (XPS). Temperature-programmed decomposition (TPDe) measurement was conducted to determine quantitatively the water, carbonate, ammonium, and nitrate residues in each HAP_m-T sample. Surface acid−base properties of the HAP_m-T samples were evaluated by temperature-programmed desorption of NH_3 (NH_3-TPD) and CO_2 (CO_2-TPD).[39] Temperature-programmed oxidation (TPO) measurements were conducted in the thermal analysis (TG/DTG) mode[40] to measure the amount of surface carbonaceous deposits on the used catalysts. Details on the instrumentation, procedures of sample pretreatment, calibration of the detector sensitivity, and quantification of the nitrogen adsorption−desorption isotherms, XPS, TPDe, TPD, and TPO measurements are given in the Supporting Information.

2.3. Catalytic Reaction, Analyses, and Quantification of the Product Mixtures. The gas-phase dehydration of LA was conducted under atmospheric pressure in a vertical fixed-bed quartz reactor of 50 cm length and 0.9 cm internal diameter placed in the center of and heated by a cylindrical electrical furnace, which is similar to the apparatus described in our earlier studies of catalytic dehydration of glycerol for acrolein production.[41,42] The catalyst (500 mg, 20−40 mesh or 0.43−0.85 mm) was sandwiched in the middle of the reactor with quartz wools. A bed of quartz sands (ca. 2 mL by volume and ca. 2 cm by height) was placed above the catalyst in order to preheat and ensure a complete evaporation of the liquid feed. Prior to the reaction, the catalyst was pretreated at the reaction temperature for 1 h in flowing dry N_2 (25 mL/min). The reaction feed, an aqueous solution containing 35.7 wt % or 10 mol % LA, was fed into the reactor using N_2 (15.5 mL/min) as the carrier gas. Unless otherwise specified, the

dx.doi.org/10.1021/cs500388x | ACS Catal. 2014, 4, 1931−1943

Table 1. Composition and Textural Properties of the HAP_m-T Samples

sample	calc. temp. (°C)	molar Ca/P ratio			SA[b] (m^2 g^{-1})	PV[c] (cm^3 g^{-1})	PD[d] (nm)
		theory[a]	XRF	XPS			
$HAP_{1.58}$-360	360	1.52	1.58	1.30	135	0.49	13.0
$HAP_{1.60}$-360	360	1.59	1.60	1.31	140	0.53	12.7
$HAP_{1.62}$-360	360	1.67	1.62	1.33	143	0.51	13.8
$HAP_{1.68}$-360	360	1.75	1.68	1.36	136	0.50	14.2
$HAP_{1.69}$-360	360	1.83	1.69	1.41	145	0.54	14.3
$HAP_{1.62}$-400	400	1.67	1.62	1.33	119	0.48	13.7
$HAP_{1.62}$-500	500	1.67	1.62	1.34	90	0.43	14.6
$HAP_{1.62}$-600	600	1.67	1.62	1.33	64	0.29	17.1
$HAP_{1.62}$-700	700	1.67	1.62	1.33	51	0.17	19.6

[a]The starting molar $Ca(NO_3)_2/(NH_4)_2HPO_4$ ratio in the preparation solution. [b]BET surface area. [c]Pore volume measured at P/P_0 = 0.995. [d]Average pore diameter measured from the desorption branch according to the BJH method.

weight hourly space velocity of LA ($WHSV_{LA}$) and reaction temperature were 2.1 h^{-1} and 360 °C, respectively. Effluents from the reactor were condensed with an ice−water trap and collected hourly for analyses with gas chromatography (GC) and ion chromatography (IC) or GC coupled with a mass analyzer (GC-MS). The details for these GC, IC, and GC-MS analyses are described in the Supporting Information.

The LA conversion, product selectivity, and yield were calculated according to the following calculations:

$$\text{LA conversion (\%)} = \frac{\text{moles of LA consumed}}{\text{moles of LA in the feed}} \times 100$$

$$\text{Product selectivity (mol \% or C \%)} = \frac{\text{moles of carbon atoms in the product defined}}{\text{moles of carbon atoms in LA consumed}} \times 100$$

$$\text{AA yield (mol \% or C \%)} = \frac{\text{moles of AA produced}}{\text{moles of LA in the feed}} \times 100$$

The catalytic activity was expressed as the area-specific catalytic rates according to consumption of LA and formation of product (AA and AD), which were obtained using the following equations:

$$\text{LA consumption rate} = \frac{\text{moles of LA consumed per hour in the reactor (mol/h)}}{\text{surface area of the catalyst in the reactor } (m^2)}$$

$$\text{Product formation rate} = \frac{\text{moles of the defined product formed per hour in the reactor (mol/h)}}{\text{surface area of the catalyst in the reactor } (m^2)}$$

3. RESULTS AND DISCUSSION

3.1. Composition, Texture, Crystallinity, and Volatile Residues of HAP_m-T Samples. Table 1 shows the composition by molar Ca/P ratio (m) and texture properties for every HAP sample prepared in this work. The composition by number m, as measured by XRF, in the HAP_m-T sample showed some derivation from the starting Ca/P ($Ca(NO_3)_2/(NH_4)_2HPO_4$) ratio in the preparation solution. The number m was slightly higher than the theoretical Ca/P ratio when the starting Ca/P ratio was lower than the stoichiometry for $Ca_{10}(PO_4)_6(OH)_2$, the stoichiometric HAP (Ca/P = 1.67), but became lower than the theoretical ratio when the starting Ca/P ratio was higher than 1.67. These results are similar to those reported in earlier literature.[36,38] According to the deficiency or excess of Ca^{2+} ions relative to the stoichiometric HAP, the HAP_m-T samples of $m \leq 1.67$ would be called Ca-deficient HAPs[32,36,43−47] while those of $m > 1.67$ would be Ca-rich HAPs.[43,44] These nonstoichiometric HAPs can be regarded as HAP with structure defects because of ion substitution by either cationic (e.g., H^+) or anionic ions (e.g., CO_3^{2-}).[43−48] Figure S1 and Table S1 in the Supporting Information show the results of XPS measurement of the surface composition for the HAP_m-T samples. Besides Ca, P, and O, a large amount of C was observed in all of the samples examined. Analysis of C 1s and O 1s peaks showed the existence of carbonates on the surface of the HAP_m-T samples, indicating some contamination with CO_3^{2-} during the precipitation.[44,45] The amount of carbonates decreased with T of the HAP_m-T sample (Table S1). Also shown in Table 1 are the XPS molar Ca/P ratios at the surface of the HAP_m-T samples. These XPS Ca/P ratios were always lower than those obtained from XRF measurements, which is the characteristic feature for HAP samples.[37,49−51]

Textural properties were derived from the nitrogen adsorption−desorption isotherms at 77 K shown in Figure S2. The surface area and pore volume of the $HAP_{1.62}$-T sample decreased, respectively, from 143 to 51 $m^2 \cdot g^{-1}$ and 0.51 to 0.17 $cm^3 \cdot g^{-1}$ with increasing the calcination temperature T. The samples of T = 360−500 °C gave similar pore diameters (ca. 14 nm), but the pores became enlarged for those samples of T > 500 °C. These results agree well with those reported by El Shafei et al.[52] The similar surface areas (ca. 140 $m^2 \cdot g^{-1}$), pore volumes (ca. 0.52 $cm^3 \cdot g^{-1}$), and pore diameters (ca. 13−14 nm) for the five HAP_m-360 samples would indicate that the variation in composition (m) of these samples had little effect on their texture properties.

The powder XRD patterns of the HAP_m-T samples, shown in Figure S3, were very characteristic of crystalline HAP (JCPDS 01−086−074); no signals for other phases like CaO and $Ca_3(PO_4)_2$ could be detected. These results demonstrate the very good thermal stability of crystalline HAPs, which is in line with the report that transformation of crystalline hydroxyapatites into mixed oxides would not happen unless they were calcined at temperatures higher than 900 °C.[53] As shown in Figure S3, the $HAP_{1.62}$-T samples of $T \leq 400$ were apparently of poor crystallinity as they gave only broad and weak diffractions. The other $HAP_{1.62}$-T samples (T > 500) gave stronger and sharper diffractions; the peak at 2θ = ca. 32° split to two peaks of 2θ = 31.77° (211) and 32.2 (112) when T was increased to 700 °C. Note that the five HAP_m-360 samples yielded very similar patterns, which are consistent with those of Tsuchida et al.,[37,38] who showed that variation of m had little effect on the crystallinity of HAP_m-360. The lattice parameters and average crystallite sizes calculated from the XRD patterns are presented in Table S2 for every HAP_m-T sample. The lattice

dx.doi.org/10.1021/cs500388x | ACS Catal. 2014, 4, 1931−1943

parameter (a) decreased with the increase in m, which is in agreement with earlier literature that a heavier CO_3^{2-}-substitution of PO_4^{3-} would happen in the sample with a higher m.[54,55]

Besides the composition by m, texture, and crystal structure, residual entities like water, ammonium cations, nitrate, and carbonate anions would also influence the surface and catalytic properties of the HAP$_m$-T samples.[53,54] These possible residual entities were probed by TPDe measurements of the HAP$_m$-T samples (Figure S4), which detected clear evolutions of H_2O below 500 °C, CO_2 and NO_2 in the temperature range of 100−800 °C, and NH_3 at above 500 °C. The signal of H_2O was the strongest, follow by that of CO_2, then those of NH_3 and NO_2. Quantitatively, water and carbonate were detected, respectively, as the main (ca. 4−5 wt %) and minor (<0.7 wt %) residues in these HAP$_m$-360 samples, and ammonium and nitrates were the insignificant residues (<0.05 wt %). The overall amount of residues became lowered with T of HAP$_{1.62}$-T, and in particular no NH_3 evolution could be detected for those samples of T > 500 °C (Table S3). These results are in line with those reported earlier by Yasukawa et al.[56]

3.2. Catalytic Performance for the LTA Reaction.

3.2.1. Methods for the Determination of LA Conversion and Product Selectivity. Many earlier studies used GC as the only tool in analyzing the condensates in the ice−water trap at the reactor outlet. Only a few studies analyzed the condensates using HPLC or GC combined with HPLC.[14,15,57] We feel obligated to alert that the results based only on GC analysis could not be that reliable for the quantification of unconsumed LA in the condensate. This problem was identified because the results from our GC analyses failed to give good material balance for the reaction (>95%) when the conversion of LA was higher than ca. 70% or when the concentration of LA in the condensate was lower than ca. 15 wt %; the material balance level for the LTA reaction was unfortunately seldom clearly reported in the literature. Considering that LA may dissociate, as a typical organic acid, into a proton (cation) and a lactate (anion) in water, and IC (ion chromatography) would be highly efficient and reliable for analyzing the lactate anions in aqueous solution,[58,59] we developed an IC analysis method for the accurate determination of lactate (LA) and acrylate (AA) in the condensates of the LTA reaction, using authentic aqueous solutions containing known amounts of LA and AA for calibrations (Figure S6, Supporting Information). To be convincing, examples are shown in Figures S7 and S8 (Supporting Information). A condensate from one test of the catalytic reaction (condensate-A) produced Figure S7A by GC analysis, which detected no LA and would seemingly report a complete consumption of LA in the reaction. Another test of the reaction (condensate-B) produced Figure S7B by GC analysis, which detected a tailing peak for LA and would seemingly report a LA conversion of 88%. However, the IC analysis results (Figure S8) showed that the LA conversion was actually 80% for condensate-A and 30% for condensate-B. The establishment of this IC analysis method enabled us to accurately determine the LA conversion and AA yield in all possible levels (0−100%). Fortunately, the GC analysis was also efficient and reliable for the determination of AA, the main product of the LTA reaction, which provided the basis to quantify the other products for selectivity measurement.

3.2.2. Effect of the Catalyst Molar Ca/P Ratio. The composition or molar Ca/P ratio (m) could be important to the catalytic performance of HAP catalysts.[32−35,37] HAP$_m$-360 samples were used to investigate the effect of m on the catalytic performance of HAP for the LTA reaction; the reaction feed was an aqueous solution of LA (molar LA/H_2O = 1/9). Figure 1 presents the time course curves of LA conversion, AA selectivity, and AA yield over these HAP$_m$-360 catalysts at 360 °C; the space velocity of LA was WHSV$_{LA}$ = 2.1 h^{-1}. The LA conversion increased more or less with the reaction time-on-stream (TOS) during the initial 2−3 h, followed by showing a decreasing trend during TOS = 3−5 h but fairly stable catalysis at longer TOS. On the other hand, the AA selectivity curves for the samples of $m \leq 1.62$ increased while the curves for those of m > 1.62 declined slightly during the early 2−3 h, and thereafter became stabilized at longer TOS. The increase in LA conversion during the initial hours of the reaction would demonstrate the existence of an induction period of 2−3 h, which could arise from a modification of the catalyst surface

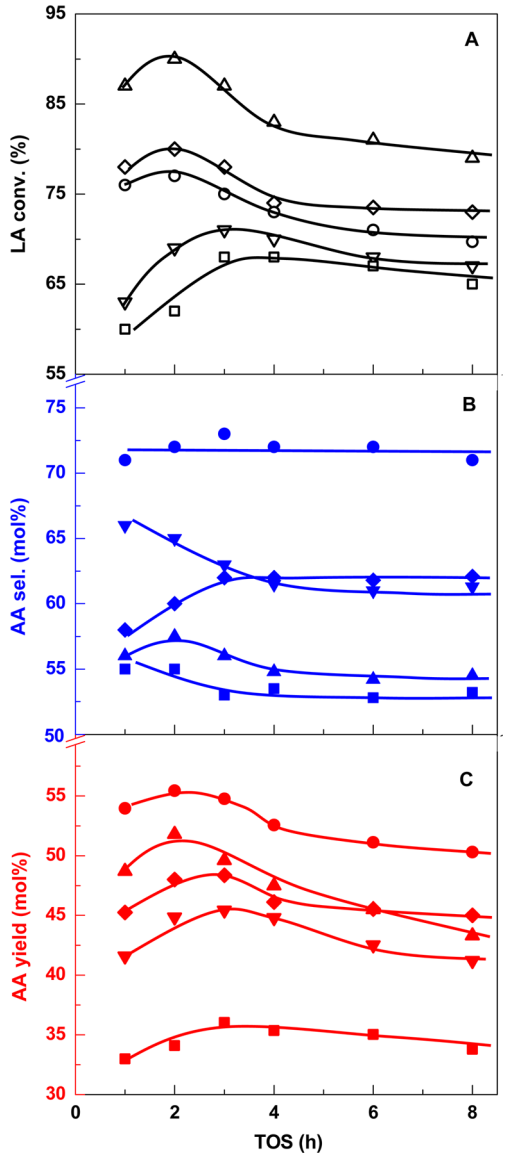

Figure 1. Performance of the HAP$_m$-360 catalysts of m = 1.58 (▲, Δ), 1.60 (♦, ◊), 1.62 (●, ○), 1.68 (▼, ▽), and 1.69 (■, □) by the time courses of LA conversion (A), AA selectivity (B), and AA yield (C). Rxn conditions: 360 °C, 7.4 kPa LA, 66.9 kPa H_2O, N_2 balance, WHSV$_{LA}$ = 2.1 h^{-1}.

dx.doi.org/10.1021/cs500388x | ACS Catal. 2014, 4, 1931−1943

Table 2. Effect of Molar Ca/P Ratio *m* on LA Conversion and Product Distribution of Catalytic LA Dehydration over the HAP_m-360 Catalysts[a]

		product selectivity (mol %)[b]									area-specific catalytic rate (μmol·h^{-1}·m^{-2})	
catalyst	LA conv. (%)	AA	AD	PA	2,3-PD	AcOH	1-HA	others[c]	AA yield (%)	carbon deposits (mg·m$_{cat}^{-2}$)[d]	LA consumption	AA formation
$HAP_{1.58}$-360	79	54	23	3	1	0	1	18	43	0.87	142	72
$HAP_{1.60}$-360	73	62	21	5	1	0	1	10	45	0.77	124	77
$HAP_{1.62}$-360	70	71	16	4	1	0	1	7	50	0.72	118	84
$HAP_{1.68}$-360	67	61	12	10	2	2	3	10	41	0.71	114	69
$HAP_{1.69}$-360	65	53	10	9	1	2	3	22	34	0.58	107	57

[a]Catalyst load, 500 mg; rxn temp., 360 °C; $WHSV_{LA}$, 2.1 h^{-1}; TOS, 6–8 h. [b]AA, acrylic acid; AD, acetaldehyde; PA, propionic acid; 2,3-PD, 2,3-pentanedione; AcOH, acetic acid; 1-HA, 1-hydroxyacetone. [c]Selectivity for "others" (mol %) = 100 − ∑(selectivity for each listed product) [d]Carbon deposits accumulated after reaction for 8 h.

Scheme 2. Possible Reactions Based on the Detected Products of LA Conversion over the Present HAP Catalysts[a]

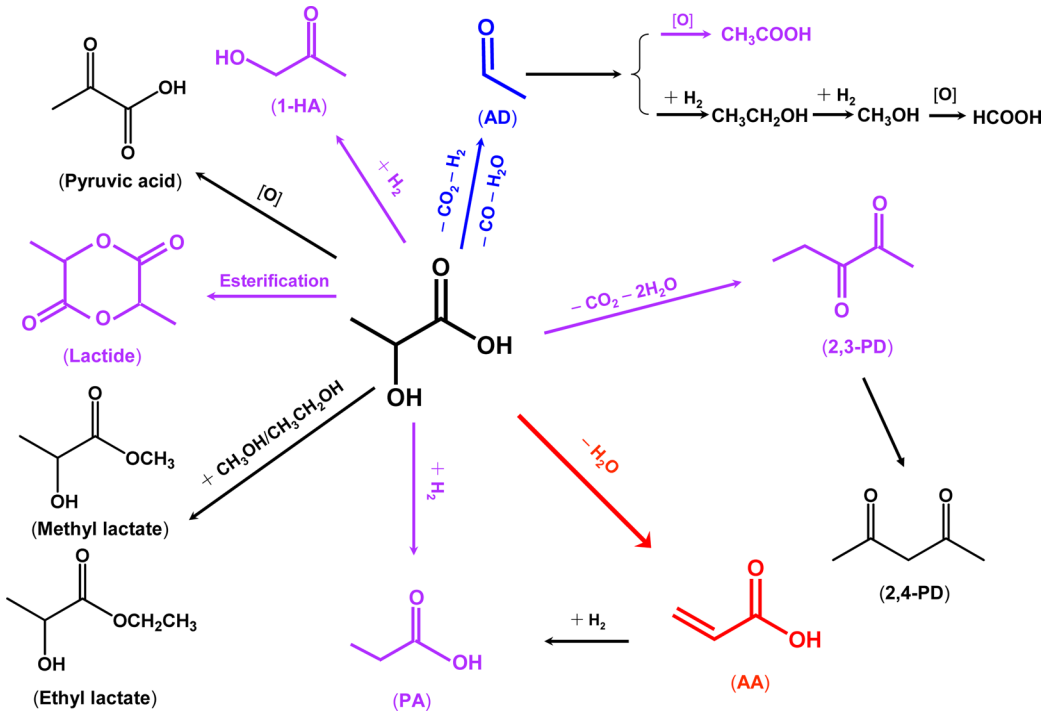

[a]The selectivity for each of the products shown in the black color was no more than 1 mol %.

(acid–base property) by steam (water) since the reaction was carried out in the presence of a very large amount of water (molar H_2O/LA = 9).[39,60,61] The LA conversion curves also showed that the sample with a lower *m* always exhibited a higher activity. The AA yield curves changed like the LA conversion curves, indicating that the decline in AA yield at longer TOS was due to catalyst deactivation. However, the $HAP_{1.62}$-360 sample (*m* = 1.62) always showed the highest selectivity and yield for producing the desirable AA, regardless of its significantly lower activity than the $HAP_{1.58}$-360 and $HAP_{1.60}$-360 samples (Figure 1B and C). The stabilized AA selectivity was as high as 71 mol %, and the AA yield at TOS = 6–8 h was 50 mol % over this best performing $HAP_{1.62}$-360 catalyst.

The catalytic reaction data obtained for TOS = 6–8 h are given in Table 2 to show the stabilized product distribution data over the HAP_m-360 catalysts. The main product was AA (selectivity: 53–71 mol %), and AD (10–23 mol %) appeared as the most abundant byproduct. Other byproducts were PA (2–10 mol %), 1-HA (1–3 mol %), 2,3-PD (1–2 mol %), and AcOH (0–2 mol %). A number of other minor byproducts (Figure S7, Supporting Information) were also detected, including lactide, ethanol, paracetaldehyde, methanol, formic acid, 2, 4-pentanedione, pyruvic acid, methyl lactate, and ethyl lactate; the selectivity for each of these individuals was always less than 1 mol % (Scheme 2). Except the clearly named products in the table, any other product including all the minor byproducts and the carbonaceous deposits formed on the catalyst surface at TOS = 6–8 h are arbitrarily added up and shown as "others" in Table 2. The overall selectivity for these "others" decreased from 18 mol % to as low as 7 mol % when *m* was increased from 1.58 to 1.62 but increased to as high as 20 mol % when *m* was further increased to 1.69. The amounts of AD and surface carbon deposits (accumulated during the reaction period of 8 h) declined while that of PA increased more or less with the increase of *m* in the HAP_m-360 catalyst. On the other hand, the variation in *m* changed the selectivity of 2,3-PD, 1-HA, and AcOH by 1–3 times though the selectivity

dx.doi.org/10.1021/cs500388x | ACS Catal. 2014, 4, 1931–1943

for each of these individual minor byproducts was produced in no more than 3 mol %. Also given in Table 2 are the area-specific catalytic rates for LA consumption and AA production during TOS = 6−8 h; the LA consumption rate decreased with the increase in m while the AA formation rate was maximized at m = 1.62 or on $HAP_{1.62}$-360.

Therefore, a comprehension of the catalytic data shown in Figure 1 and Table 2 would identify $HAP_{1.62}$-360 as the best performing catalyst for production of AA from LA, which gave the highest AA selectivity (71 mol %) and AA yield (50 mol %), as well as the lowest selectivity for the "others" (7 mol %). The precursor of this $HAP_{1.62}$-360 (a dry $HPA_{1.62}$) is then used in the following to investigate the effect of T, another significant factor affecting the catalytic performance of HAP catalysts.[62,63]

3.2.3. Effect of the Calcination Temperature. Figure 2 shows the variation in T (360−700 °C) of $HAP_{1.62}$-T on the time course curves of LA conversion, AA selectivity and AA yield of the LTA reaction. These time course curves were generally similar to those in Figure 1. Regardless of TOS, both the LA conversion (Figure 2A) and AA selectivity (Figure 2B) declined steadily with the increase in T of the catalyst sample, resulting in significantly lowered AA yield over the sample of a higher T (Figure 2C). These could be due to that the increase in T enhanced crystallization degree (Figure S3, Supporting Information) and lowered the specific surface area of the sample (Table 1) and reduced the number of active surface sites (see section 3.3). The AA selectivity and yield levels over $HAP_{1.62}$-600 and $HAP_{1.62}$-700 were reduced to as low as 29−30 mol % and 8−15 mol %, which corresponded, respectively, only to a half and a quarter of their corresponding levels obtained over the $HAP_{1.62}$-360 catalyst (see also Table 3).

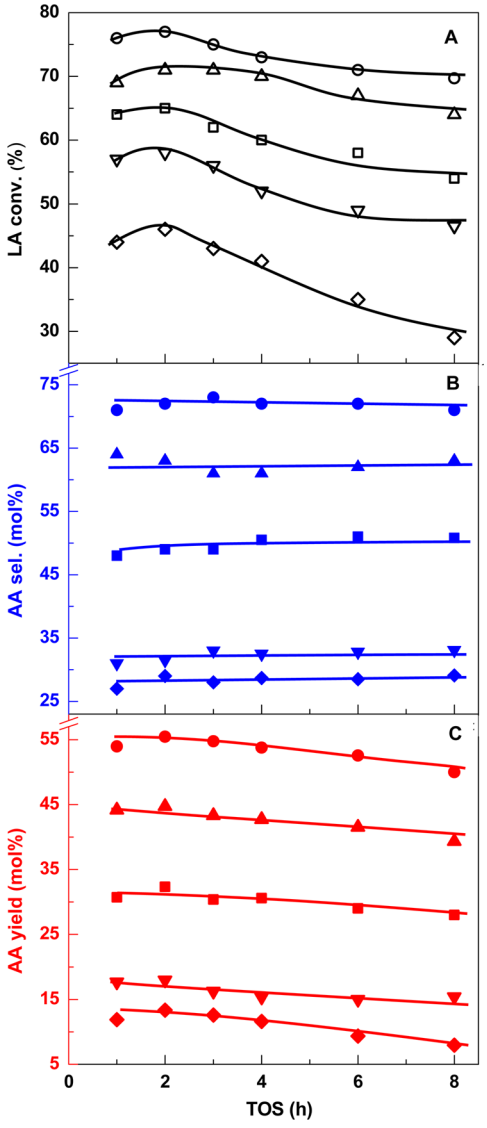

Figure 2. Performance of the $HAP_{1.62}$-T catalysts of T = 360 °C (●, ○), 400 °C (▲, △), 500 °C (■, □), 600 °C (▼, ▽), and 700 °C (♦, ◊) by the time courses of LA conversion (A), AA selectivity (B), and AA yield (C). Rxn conditions: 360 °C, 7.4 kPa LA, 66.9 kPa H_2O, N_2 balance, $WHSV_{LA}$ = 2.1 h^{-1}.

The lowered AA selectivity and yield on increasing T of the $HAP_{1.62}$-T catalyst indicate more byproducts formation over the catalyst of a higher T. Table 3 reports the effects of T on the stabilized product distribution data (measures at TOS = 6−8 h) and the amounts of surface carbon deposited on the $HAP_{1.62}$-T catalysts during the reaction period of 8 h. Similar to the T effect on the AA selectivity, increasing T of the $HAP_{1.62}$-T catalyst increased the amount of surface carbon deposits by 10−15%, lowered the selectivity for AD and PA, but had little effect on the selectivity for the other byproducts (2,3-PD, 1-HA, and AcOH). On the other hand, the overall selectivity for "others" increased significantly with T of the $HAP_{1.62}$-T catalyst; these "others" were doubled and then redoubled when T was increased from 360 to 400 °C and then 500 °C and became 7−8 times that over $HAP_{1.62}$-360 (7 mol %) at T = 600 and 700 °C. It should be mentioned that these "others" over the $HAP_{1.62}$-T catalysts of $T \geq$ 500 °C included also a water-insoluble substance, whose amount increased with T increasing from 500 to 700 °C. This insoluble substance was separated from the condensates by filtration and washing with water and then dissolved in DMF and subjected to GC-MS analysis to identify its chemical identity. The analysis showed one dominating peak in the chromatogram, which was identified by MS as lactide (m/z = 144), the cyclic diester of LA. Formation of lactide was also detected very recently from the reaction of LA over other phosphate catalysts.[14,16] The area-specific LA consumption rate increased from 0.118 to 0.143 mmol h^{-1} m^{-2} with T increasing from 360 to 500 °C but was lowered to 0.125 mmol h^{-1} m^{-2} when T was further increased to 700 °C. In parallel with the AA selectivity changes, the AA formation rate, however, decreased steadily with the T increasing because the side reactions, especially those responsible for the formation of "others" including lactide, became more severe over the catalyst prepared with a higher T.

Thus, the results of Figures 1 and 2 clearly identify $HAP_{1.62}$-360 as the most efficient HAP catalyst for the LTA reaction. This $HAP_{1.62}$-360 catalyst is then used below to study the effects of reaction temperature and of space velocity of LA ($WHSV_{LA}$) on the catalytic LTA performance.

3.2.4. Effect of the Reaction Temperature. Figure 3 shows the reaction temperature effect on the time course curves of LA conversion, AA selectivity, and AA yield over the $HAP_{1.62}$-360 catalyst in the temperature range of 340 to 380 °C. As would be anticipated, the increase of the reaction temperature from 340 to 380 °C resulted in continued increase of the LA conversion during the reaction period of 8 h, regardless of TOS. On the other hand, the stabilized selectivity for the desirable AA (TOS = 6−8 h) was maximized to 71 mol % when the reaction temperature was 360 °C; the use of either a lower or higher

dx.doi.org/10.1021/cs500388x | ACS Catal. 2014, 4, 1931−1943

Table 3. Effect of Calcination Temperature T on LA Conversion and Product Distribution of Catalytic LA Dehydration over the $HAP_{1.62}$-T Catalysts[a]

		product selectivity (mol %)									area-specific catalytic rate (μmol·h^{-1}·m^{-2})	
catalyst	LA conv. (%)	AA	AD	PA	2,3-PD	AcOH	1-HA	others	AA yield (%)	carbon deposits (mg·m$_{-cat}^{-2}$)[b]	LA consumption	AA formation
$HAP_{1.62}$-360	70	71	16	4	1	0	1	7	50	0.72	118	84
$HAP_{1.62}$-400	63	62	14	4	2	1	2	15	39	0.72	126	78
$HAP_{1.62}$-500	54	51	13	3	1	0	1	31	28	0.87	143	69
$HAP_{1.62}$-600	46	33	13	1	0	0	2	51	15	0.82	138	57
$HAP_{1.62}$-700	29	29	11	1	1	0	3	55	8	0.79	125	55

[a]Reaction conditions: see the footnote of Table 2. [b]Carbon deposits accumulated after reaction for 8 h.

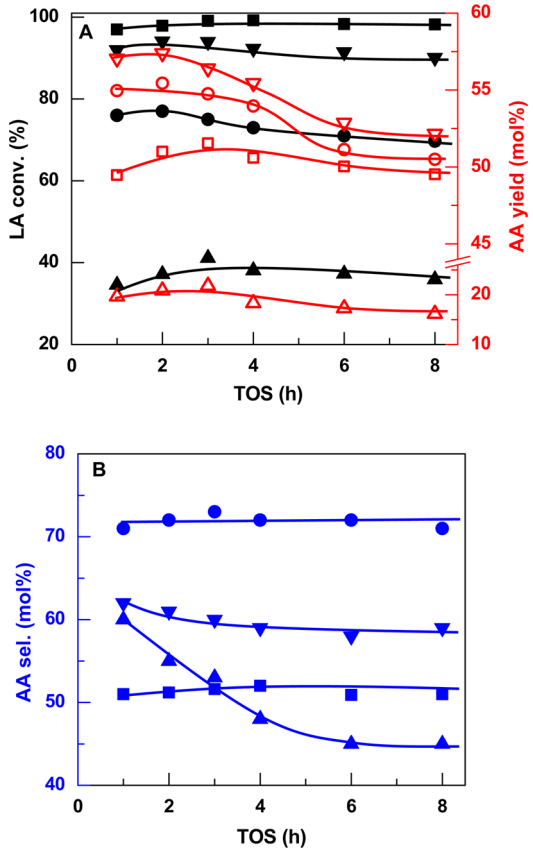

Figure 3. Effect of reaction temperature on the catalytic performance of $HAP_{1.62}$-360 by the time courses of LA conversion and AA yield (A) and AA selectivity (B). Rxn temp.: 340 °C (▲, △), 360 °C (●, ○), 370 °C (▼, ▽), 380 °C (■, □). Other conditions: 7.4 kPa LA, 66.9 kPa H_2O, N_2 balance, $WHSV_{LA}$ = 2.1 h^{-1}.

temperature (e.g., 340 or 370 °C) for the reaction would result in significantly lower AA selectivity. However, the stabilized AA yield appeared similar (ca. 50 mol %, Table 4) when the reaction temperature was in the range of 360−380 °C due to the decreased AA selectivity at a higher temperature being compensated by an increase in the LA conversion. The optimum reaction temperature for the LTA reaction would therefore be 360 °C as the AA selectivity obtained at this temperature was distinctly higher (Figure 3B); the use of either higher and lower reaction temperatures would significantly lower the utilization efficiency of LA or lead to a large amount of unwanted products (waste), though the use of a slightly higher temperature (e.g., 370 °C) would not change the AA yield.

The data obtained at 370 and 380 °C in Figure 3 might be questioned as these temperatures exceeded the calcination temperature of the catalyst $HAP_{1.62}$-360 (T = 360 °C). The $HAP_{1.62}$-400 catalyst was then used to check the reaction temperature effect on the product selectivity; the results (Figure S9, Supporting Information) clearly confirm that 360 °C was indeed the optimum reaction temperature for offering the highest AA selectivity, distinctly higher than those numbers obtained at either a lower (345 °C) or a higher temperature (375 °C). Though the highest AA yield (48 mol %) was obtained at 375 °C over this $HAP_{1.62}$-400 catalyst, this highest AA yield was still no higher than the yield offered by $HAP_{1.62}$-360 at 360 °C (50 mol %).

The detailed product distribution data at TOS = 6−8 h over the $HAP_{1.62}$-360 catalyst at the different temperatures are presented in Table 4. Due to a significant formation of lactide, the selectivity for the "others" (43 mol %) at the lowest temperature (340 °C) became comparable to that for the desirable AA, much higher than those obtained when the reaction temperature was no lower than 360 °C (7−20 mol %). Interestingly, the formation of lactide was not detected and the selectivity for "others" was minimized at 360 °C. Besides a

Table 4. Effect of Reaction Temperature on LA Conversion and Product Distribution of Catalytic LA Dehydration over $HAP_{1.62}$-360[a]

		product selectivity (mol %)									area-specific catalytic rate (μmol·h^{-1}·m^{-2})	
Rxn temp. (°C)	LA conv. (%)	AA	AD	PA	2,3-PD	AcOH	1-HA	others	AA yield (%)	carbon deposits (mg·m$_{-cat}^{-2}$)[b]	LA consumption	AA formation
340	37	45	8	3	0	0	1	43	17	0.48	62	28
360	70	71	16	4	1	0	1	7	50	0.72	118	84
370	89	58	18	4	1	1	2	16	52	1.02	150	85
380	98	51	19	5	1	0	2	22	50	1.35	165	84

[a]Catalyst load, 500 mg; $WHSV_{LA}$, 2.1 h^{-1}; TOS, 6−8 h. [b]Carbon deposits accumulated after reaction for 8 h.

dx.doi.org/10.1021/cs500388x | ACS Catal. 2014, 4, 1931−1943

slight increase in the PA selectivity, increasing the reaction temperature significantly enhanced the selectivity of AD, indicating that the decarbonylation or decarboxylation reaction of LA could happen more easily at a higher reaction temperature.[11−14] The present observations on the effect of reaction temperature are consistent with those of Lin et al.[11] who studied the LTA reaction over calcium sulfate catalysts promoted with cupric sulfate and phosphates. Note that the present observation on maximizing the selectivity for the desired AA coincided with the minimization of the selectivity for "others" in Table 4 at 360 °C. This coincidence strongly makes 360 °C the optimum reaction temperature for the LTA reaction over HAP catalysts. That is also why this present work has made 360 °C the standard reaction temperature for the LTA reaction over the HAP$_m$-*T* catalysts.

3.2.5. Effect of the LA Space Velocity (WHSV$_{LA}$). Figure 4 shows the effect of WHSV$_{LA}$ on the catalytic performance of

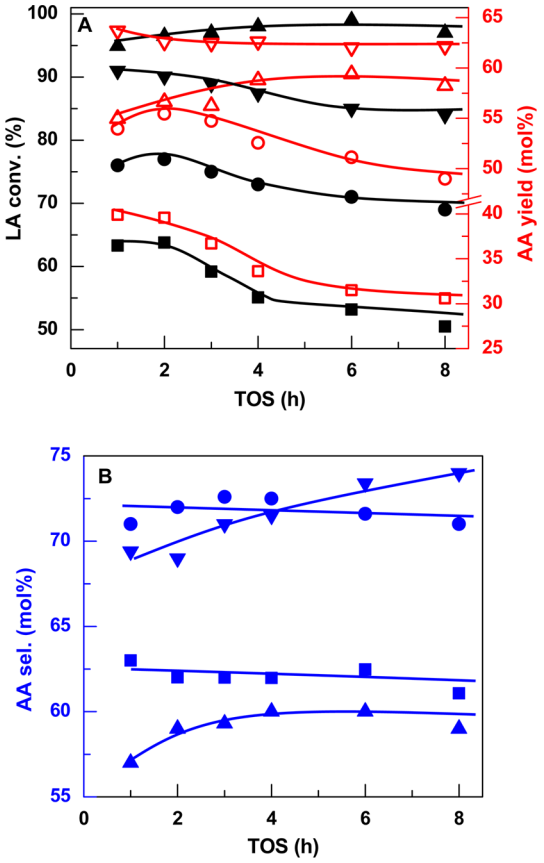

Figure 4. Effect of WHSV$_{LA}$ on the catalytic performance of HAP$_{1.62}$-360 by the time courses of LA conversion and AA yield (A) and AA selectivity (B). WHSV$_{LA}$: 0.7 h^{-1} (▲, △), 1.4 h^{-1} (▼, ▽), 2.1 h^{-1} (●, ○), 2.8 h^{-1} (■, □). Other conditions: 360 °C, 7.4 kPa LA, 66.9 kPa H_2O, N_2 balance.

HAP$_{1.62}$-360 by the time course curves of LA conversion and AA selectivity at 360 °C. The variation of WHSV$_{LA}$ (0.7−2.8 h^{-1}) was done by changing the introduction rate of the reaction feed between 1 and 4 mL/h. As would be anticipated, increasing the WHSV$_{LA}$ from 0.7 h^{-1} to 2.8 h^{-1} resulted in a steady lowering of the LA conversion. Also, the catalyst deactivation became significantly faster when WHSV$_{LA}$ of the reaction became higher than 2.1 h^{-1}, which could be due to bimolecular side reactions leading to carbon deposits becoming more severe at higher WHSV$_{LA}$. The variation of WHSV$_{LA}$ produced a significant effect on the selectivity for the formation of the desirable AA (Figure 4B), which clearly reveals that the optimum window of WHSV$_{LA}$ for the selective production of AA would be between 1.4 and 2.1 h^{-1}. For up to TOS = 8 h, the AA selectivity in this window was maintained as high as 71−74 mol %; either increasing or lowering the WHSV$_{LA}$ from this window would significantly lower the selectivity for AA production. The stable AA yield during the reaction (TOS = 4−8 h) increased from ca. 57 mol % to ca. 62 mol % on increasing the WHSV$_{LA}$ from 0.7 to 1.4 h^{-1}. However, the AA yield kept on decreasing during the reaction when the WHSV$_{LA}$ was further increased to 2.1 and 2.8 h^{-1}, giving a yield of 51 mol % and 34 mol %, respectively, at TOS = 6−8 h. The higher AA yield at WHSV$_{LA}$ = 0.7 h^{-1} than at WHSV$_{LA}$ = 2.1 h^{-1} was apparently due to the use of the smallest WHSV$_{LA}$ always being able to produce far higher LA conversion. This combination of the low AA selectivity (<60 mol %) with the high LA conversion (>95%) for yielding AA during the reaction at WHSV$_{LA}$ = 0.7 h^{-1} would also mean low utilization efficiency of LA or formation of a large amount of waste products.

Presented in Table 5 are the detailed product distribution data at TOS = 6−8 h over the HAP$_{1.62}$-360 catalyst at the various WHSV$_{LA}$. It is observed that the variation of WHSV$_{LA}$ significantly affected the formation of "others," besides the formation of the desired AA; the selectivity for these "others" in the optimum WHSV$_{LA}$ window (1.4−2.1 h^{-1}) for the selective AA production was as low as 2−7 mol % but became higher than 19 mol % outside the window. The considerably higher selectivity of "others" at the lower and higher ends of WHSV$_{LA}$ could mean differently. At the lower end (WHSV$_{LA}$ = 0.7 h^{-1}), the secondary reactions (such as decomposition) of AA and other products would become more preferred due to their increased residence time in the reactor. At the higher end (WHSV$_{LA}$ = 2.8 h^{-1}), evaporation of the reaction feed could become more or less insufficient, which could induce more noncatalytic thermal reaction on the heating quartz sands and/or lead to locally enriched LA for polymerization and coking.

Therefore, the catalytic data presented in this section point to HAP$_{1.62}$-360 being the best performing catalyst for the LTA reaction, which could offer an AA yield of 50−62% (AA selectivity 71−74 mol %) under the optimum reaction conditions (temperature 360 °C, WHSV$_{LA}$= 1.4−2.1 h^{-1}).

3.3. Acid−Base Properties of HAP$_m$-*T*. Measurements of NH_3- and CO_2-TPD were done to evaluate the acid−base property of the HAP$_m$-*T* samples. Since both NH_3 and CO_2 could be generated from the thermal decomposition of the as-prepared HAP$_m$-*T* samples (e.g., Figure S4), blank experiments were also conducted to identify and measure the evolutions of NH_3 and CO_2 during temperature-programmed heating of each HAP$_m$-*T* sample. For example, the curves (c′) in Figure 5 show the evolutions of NH_3 in the temperature range of 380−600 °C (Figure 5A) and CO_2 in the range of 360−800 °C (Figure 5B) from the blank HAP$_{1.62}$-360 sample; no evolution of NH_3 or CO_2 was detected below 360 °C because the sample had been purged at 360 °C with flowing Ar during the pretreatment, simulating the sample pretreatment in the catalytic reactor prior to the LTA reaction. These blank "TPD" measurements enable us to assign the signals at above 360 °C in Figure 5 to the evolutions of NH_3 or CO_2 from the thermal decomposition of ammonium or carbonate residues in the HAP$_m$-360 samples. Thus, the integration of the TPD peaks in the temperature range below 360 °C was done to quantify the amount of

dx.doi.org/10.1021/cs500388x | *ACS Catal.* 2014, 4, 1931−1943

Table 5. Effect of Space Velocity of LA ($WHSV_{LA}$) on LA Conversion and Product Distribution of Catalytic LA Dehydration over $HAP_{1.62}$-360[a]

		product selectivity (mol %)									area-specific catalytic rate ($\mu mol \cdot h^{-1} \cdot m^{-2}$)	
$WHSV_{LA}$ (h^{-1})	LA conv. (%)	AA	AD	PA	2,3-PD	AcOH	1-HA	others	AA yield (%)	carbon deposits ($mg \cdot m_{-cat}^{-2}$)[b]	LA consumption	AA formation
0.7	97	59	15	4	1	1	1	19	57	0.51	55	32
1.4	84	74	18	3	1	1	1	2	62	0.63	95	70
2.1	70	71	16	4	1	0	1	7	50	0.72	118	84
2.8	50	61	12	4	1	0	2	20	31	0.82	113	69

[a]Catalyst load, 500 mg; Rxn temp., 360 °C; TOS, 6−8 h. [b]Carbon deposits accumulated after reaction for 8 h.

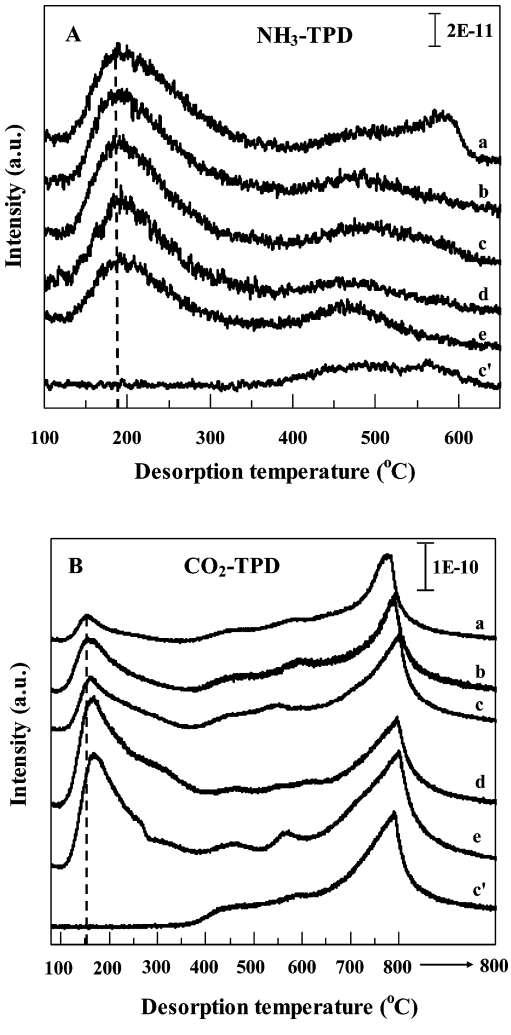

Figure 5. NH_3 (A) and CO_2 (B) TPD profiles from HAP_m-360 of m = 1.58 (a), 1.60 (b), 1.62 (c), 1.68 (d), and 1.69 (e). (c′) shows blank experimental results of $HAP_{1.62}$-360 (without adsorption of NH_3 or CO_2).

adsorbed NH_3 or CO_2 molecules at the acidic sites or basic sites.

As seen in Figure 5A, the NH_3-TPD profiles from the five HAP_m-360 samples appeared qualitatively similar, featuring only one distinct peak at ca. 190 °C regardless of the composition by m. The peak position shifted toward slightly lower temperatures (from 193 to 186 °C) while the peak area became more or less smaller when the sample composition m was increased from 1.58 to 1.69. These HAP_m-360 samples also produced similar CO_2-TPD profiles (Figure 5B), showing mainly one tailing peak at ca. 160 °C. Unlike the NH_3-TPD peak, the position of this CO_2-TPD shifted toward higher temperatures (from 152 to 167 °C), and the area of this CO_2-TPD peak became enlarged when the sample composition m was increased from 1.58 to 1.69. Moreover, the $HAP_{1.68}$-360 sample also showed a minor peak (shoulder) at ca. 310 °C and the $HAP_{1.69}$-360 sample two minor peaks (shoulders) at ca. 260 and 320 °C. These results indicate that the HAP_m-360 sample with a higher m would be weaker in acidity but stronger in basicity.

NH_3- and CO_2-TPD profiles from the $HAP_{1.62}$-T samples are given in Figure S10. The signals detected at above 360 °C were again due to the decomposition of structural and/or surface residues that were produced during the preparation or storage in ambient air of the sample, being similar to the cases of Figure 5; the continued weakening of these signals with the elevation of T in the $HAP_{1.62}$-T sample is due to such residues retained in the sample decreasing with the elevation of T (Figure S10). All five of the $HAP_{1.62}$-T samples showed only a single NH_3-TPD peak below 360 °C; the peak temperature (ca. 190 °C) lowered slightly but the peak area declined significantly when T of the sample was elevated from 360 to 700 °C (Figure S10A). The CO_2-TPD profiles from the five $HAP_{1.62}$-T samples also gave a single tailing peak below 360 °C; the peak temperature lowered a little (from 160 to 155 °C), but the peak area lowered significantly when T was elevated from 360 to 700 °C (Figure S10B). These data clearly demonstrate that both the acidity and basicity of the $HAP_{1.62}$-T sample were slightly weakened on elevation of T.

Figure 6 shows the density of surface acidic (surface acidity) and basic sites (surface basicity), which were obtained by normalizing to the sample surface area the numbers of adsorbed NH_3 and CO_2 molecules, measured respectively from the NH_3- and CO_2-TPD peaks in the temperature range of 100−360 °C (Figures 5 and S10). For the HAP_m-360 samples, the surface acidity decreased from 1.60 to 0.92 $\mu mol/m^2$ while the surface basicity increased from 0.23 to 0.68 $\mu mol/m^2$ when m was increased from 1.58 to 1.69 (Figure 6A). For the $HAP_{1.62}$-T samples, however, the surface acidity was maximized on the sample of T = 500 °C while the surface basicity was almost not affected by the T variation.

Hall et al. studied earlier the effects of molar Ca/P ratio (m) and calcination temperature (T) on the acid−base property of HAP by comparing the UV−vis absorption spectra of their adsorbed Hammett indicators.[32] They detected strongly acidic sites ($H_0 \leq -6.6$) only on the samples with relatively low molar Ca/P ratios (m = 1.57−1.60) and calcination temperatures (180−290 °C). Medium to weakly acidic sites ($-6.6 \leq H_0 \leq +0.82$) were detected on the sample with a high Ca/P ratio (1.67) or that experienced a high calcination temperature (500

dx.doi.org/10.1021/cs500388x | ACS Catal. 2014, 4, 1931−1943

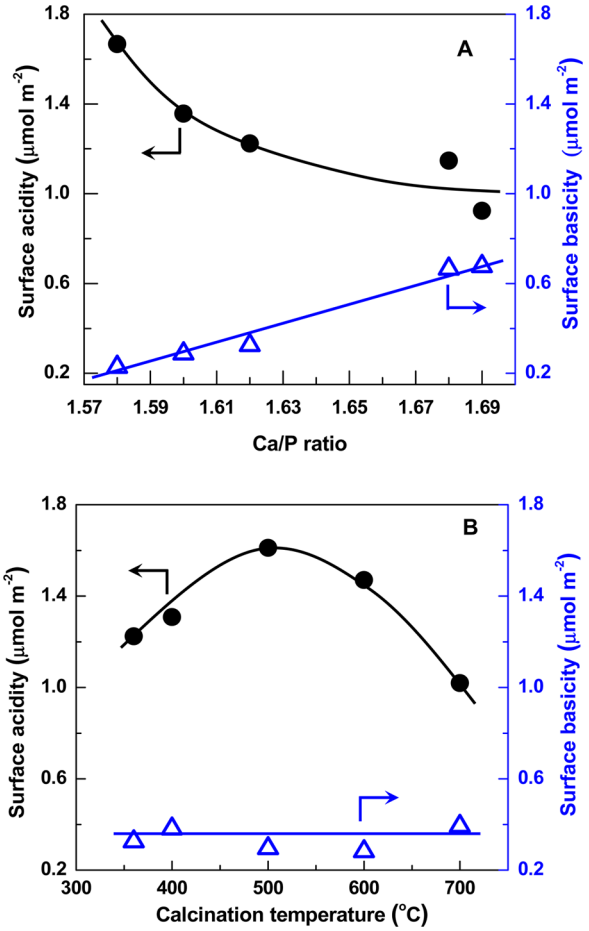

Figure 6. Effect of molar Ca/P ratio m (A) and calcination temperature T (B) on the surface acidity and basicity of HAP_m-T samples.

°C). They also showed that the number of surface acidic sites would be lowered on increasing the Ca/P ratio and/or elevating the calcination temperature from 180 to 500 °C. These earlier data are qualitatively in good agreement with the present acidity data determined from the NH_3-TPD measurements.

3.4. Correlation between the Acid−Base Property and Catalytic Performance of the HAP_m-T Samples. It has been known that the catalytic dehydration rate of alcohol over a solid oxide catalyst would be dependent on the catalyst surface acid−base property.[64] The effects of m and T on the catalytic performance of HAP_m-T (Figures 1 and 2) could thus be related to the changes in the catalyst surface acidity and basicity. An attempt is then made to correlate the rates of LA consumption and product (AA and AD) formation with the surface acidity and basicity of the HAP_m-T catalysts, obtained from NH_3- and CO_2-TPD measurements (Figure 6). The area-specific catalytic LA consumption rates were plotted in Figure S11 against the catalyst surface acidity and basicity, respectively. It appears that the LA consumption rate increased linearly with the surface acidity but decreased roughly linearly with the surface basicity.

Correlations of the area-specific AA and AD formation rates with the catalyst surface acidity and basicity are made in Figure S12. It is clear that the AD formation rate increased linearly with increasing the catalyst surface acidity but decreased with the catalyst surface basicity. On the other hand, the AA formation rate showed a volcano-type dependence either on the catalyst surface acidity or the basicity; the maximum AA formation rate was measured on the catalyst whose surface acidity and basicity were 1.1−1.3 μmol/m^2 and 0.3−0.4 μmol/m^2, respectively.

The increase with the surface acidity and decrease with the surface basicity of the AD formation rate agree qualitatively with many earlier reports.[18,19,25−31] Katryniok et al.[65] investigated the gas-phase decarbonylation of LA for AD formation over various silica-supported heteropolyacid catalysts. Without reporting their measured acidity, these authors claimed that strongly acidic silicotungstic and phosphotungstic acids offered higher activity and selectivity than the less acidic phosphomolybdic and vanado-phosphomolybdic acids for AD formation. The catalytic data gained in this work (Tables 2, 3, 4, and 5) clearly demonstrate that the lowering in the AD selectivity during the reaction was always far less than the increase in the AA selectivity; the catalytic AA formation rate was 2−5 times higher than the AD formation rate even though the surface acidity was 1.5−5 times higher than the surface basicity for these HAP_m-T catalysts. These observations imply that discrimination between the catalytic surface acidic and basic sites on HAP_m-T by the competing reactions for the selective AA and AD formation would not be possible.

Since the areal-specific LA consumption rate showed totally different dependences on the catalyst surface acidity and basicity of the present HAP_m-T catalysts (Figure S11, Supporting Information) and both the surface acidic and basic sites would be necessary for the production of AA (Figure S12, Supporting Information), an attempt is made in Figure 7 to correlate the catalytic rates at 360 °C (Tables 2 and 3) with the ratio of acidity-to-basicity (acidity/basicity). It is seen that both the LA consumption and AD formation rates increased linearly with the increase in this acidity/basicity ratio. However, the AA production rate showed a volcano-type dependence on this acidity/basicity ratio; the maximum AA production rate appeared when the catalyst surface was populated with a proper ratio of acidity/basicity (3.0−4.5). This volcano-type dependence indicates that both surface acidic and basic sites would be involved in the selective formation of AA over the HAP_m-T catalysts. In other words, the existence of an optimal ratio between the catalyst surface acidity and basicity would imply that a kind of balance between the surface acidity and basicity or cooperative acid−base catalysis was operating in directing the dehydration of LA toward the formation of AA. A very recent publication of Blanco et al. also discovered that the AA selectivity correlated well with the acid/base balance (also defined as the ratio of acidity-to-basicity ratio) on the surfaces of various phosphate catalysts.[16] Having an acidity/basicity ratio of 3.7, the $HAP_{1.62}$-360 catalyst offered the highest AA formation rate (83 μmol·h^{-1}·m^{-2}) among all HAP_m-T samples (see also Tables 2 and 3). This further identifies $HAP_{1.62}$-360 as the most efficient or best performing HAP_m-T catalyst for the LTA reaction since this catalyst also produced the highest AA selectivity during the reaction (Figures 1 and 2).

Scheme 3 is then proposed to account for the cooperative acid−base catalysis for the selective LTA reaction over the HAP_m-T catalysts. The reactant LA would be activated by interaction of its carboxyl group with the surface basic (phosphate oxygen atoms) and acidic (Ca^{2+} ions) sites, leading to acidic OH and Ca^{2+}-associated lactate (I) on the catalyst surface. The formation of lactate (I) during the reaction was believed to be the key to the selectivity for AA production in

dx.doi.org/10.1021/cs500388x | ACS Catal. 2014, 4, 1931−1943

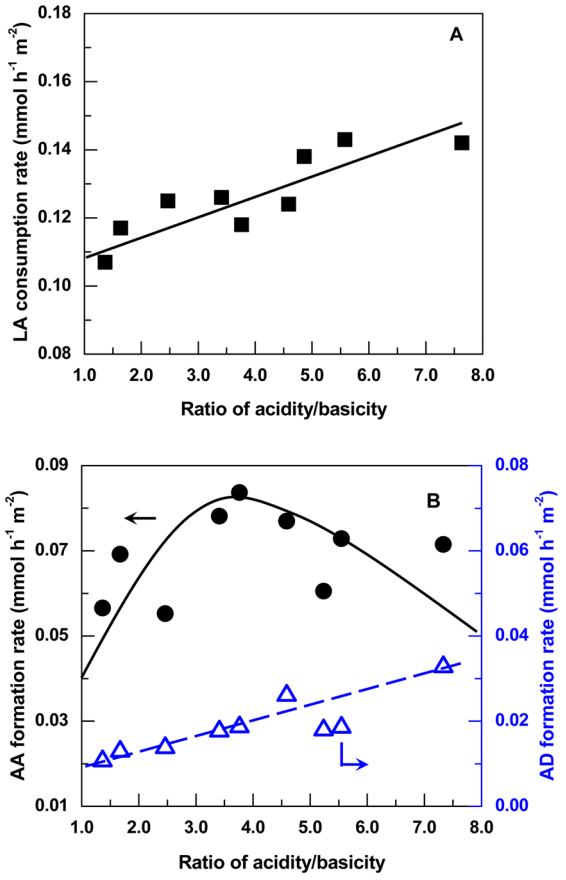

Figure 7. Dependences of the area-specific catalytic rates of LA consumption (A), and AA and AD formation (B) on the surface acidity/basicity ratio of HAP_m-*T* catalysts.

the earlier publications,[13,16,19−23] as it also served to stabilize and prevent the carboxyl group from entering the decarboxylation/decarbonylation channel leading to AD formation (Scheme 1).[13,14,16,25] Infrared spectroscopy studies of the LA conversion on phosphate[16,18] or HAP[13] catalysts had confirmed that a surface lactate species was indeed generated in the reaction. As depicted in structure II of Scheme 3, the cooperative acid−base catalysis would operate on promoting the dehydration of the surface lactate to form surface acrylate (III);[13] its desorption from the catalyst surface closes the catalytic cycle for AA formation.

3.5. Carbonaceous Deposits on the Used Catalyst and Possibility of Catalyst Regeneration. Considerable surface carbonaceous deposits were registered on the used HAP_m-*T* catalysts (e.g., Tables 2, 3, 4 and 5), which would be responsible for the observed catalyst deactivation (Figures 1, 2, 3 and 4). The deposits were quantitatively measured by TPO experiments in the thermal gravimetric analysis (TG/DTG) mode (Supporting Information). The TPO-TG/DTG curves of the used $HAP_{1.62}$-360 catalyst are presented, as an example, in Figure S13 (Supporting Information); the amount of carbonaceous deposits was measured as the weight loss in the temperature range of 250−600 °C. The amounts of carbon deposits normalized to the catalyst surface area ($mg \cdot m^{-2}$) appeared to increase with the ratio of acidity/basicity of the HAP_m-*T* catalysts (Figure S14, Supporting Information). Therefore, the catalyst featuring a higher surface acidity/basicity ratio would also induce more severe coking and faster deactivation, besides improving the formation of byproduct AD.

Element analysis, XRD and XPS measurements were conducted to characterize the used HAP_m-*T* catalysts. The measured H/C ratio in the surface carbonaceous deposits was as low as H/C = 0.42−0.59, which indicates that the carbonaceous deposits were probably formed as polyaromatic surface species.[66] The XRD measurements detected no signal for graphic carbon on the used catalysts (Figure S15, Supporting Information), revealing that the carbonaceous deposits were amorphous. The measured XPS spectra (Figure S16, Supporting Information) uncovered that these amorphous carbonaceous deposits were composed of carbon atoms in aromatic rings, carboxylate, ester, carbonate and etc., which

Scheme 3. Possible Mechanism for AA Production from LA over the HAP_m-*T* Catalysts

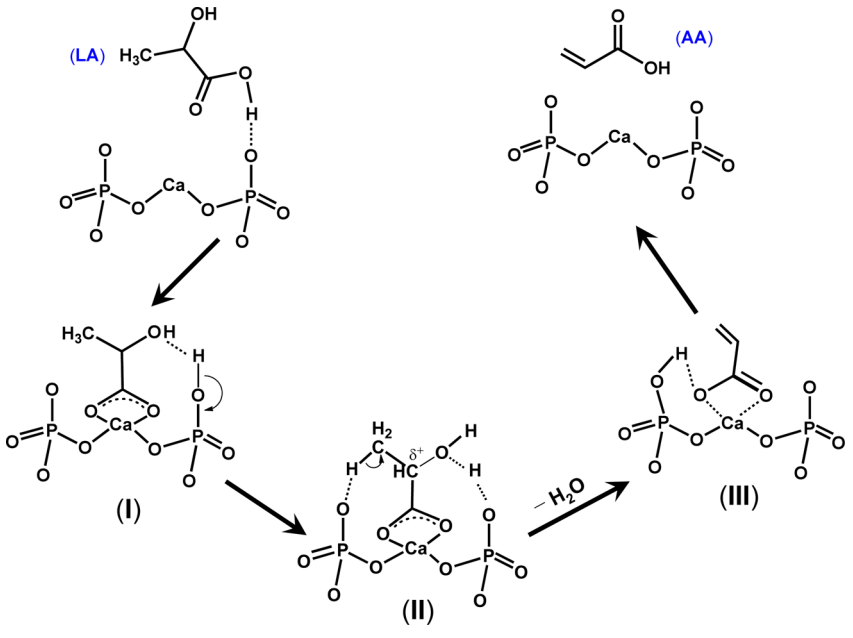

dx.doi.org/10.1021/cs500388x | ACS Catal. 2014, 4, 1931−1943

could arise from consecutive reactions of the products or complicate side reactions between the reactant and products including unidentified byproducts. Nevertheless, it is found that a simple exposure of the coked HAP_m-T catalysts to a flowing air (50 mL/min) at the reaction temperature (360 °C) for 12 h was sufficient for a full regeneration of the reacted HAP_m-T catalysts, as shown in Figure 8 for $HAP_{1.62}$-360, which could be important in view of application.

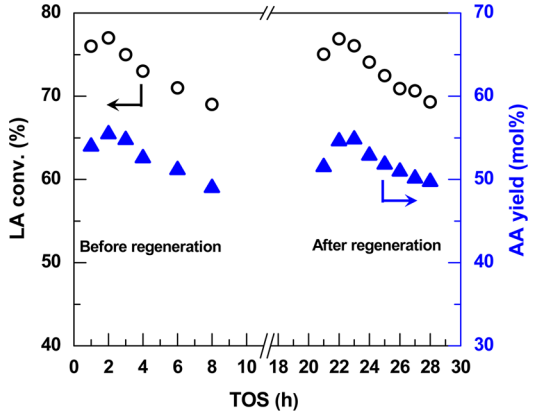

Figure 8. Deterioration-regeneration performance by the time courses of LA conversion and AA yield of $HAP_{1.62}$-360 catalyst. The fresh catalyst was reacted for 8 h and then switched to an air flow (50 mL/min) for 12 h to in situ regenerate the catalyst, followed by switching back to the reaction feed for further reaction. Rxn conditions: 360 °C, 7.4 kPa LA, 66.9 kPa H_2O, N_2 balance, $WHSV_{LA}$ = 2.1 h^{-1}.

4. CONCLUSIONS

This work demonstrates that a properly prepared HAP catalyst with a suitable composition can be efficient for the selective production of AA from LA. The molar Ca/P ratio and calcination temperature are shown to be the keys to the catalytic performance; the sample with the molar ratio of Ca/P = 1.62 and the calcination temperature of 360 °C is identified as the best performing catalyst in terms of the AA selectivity and yield. Under the optimized reaction conditions (360 °C, $WHSV_{LA}$= 1.4−2.1 h^{-1}), the selectivity and yield for AA production from LA dehydration could be as high as 71−74 mol % and 50−62%, respectively. AD produced from the acid-catalyzed decarboxylation/decarbonylation reaction of LA is identified as the main byproduct. The catalytic performance is shown to correlate strongly with the ratio of acidity/basicity at the catalyst surface. The AA formation rate shows a volcano-type dependence on this acidity/basicity ratio, which indicates that a kind of cooperative acid−base catalysis could operate during the dehydration of LA toward the formation of AA. The HAP catalysts showed more or less deactivation during the reaction but a switch to a flowing air of the reacted ones at the reaction temperature could in situ fully regenerate the catalysts for the reaction.

■ ASSOCIATED CONTENT

Supporting Information

Details on the instrumentation; procedures of sample pretreatment; calibration of the detector sensitivity and quantification of the nitrogen adsorption−desorption isotherms; XPS, TPDe, TPD, and TPO measurements; details on GC, IC, and GC-MS analyses; GC and IC profiles of two example samples of the reaction condensate and reference solution of LA and AA; the correlation between acidity density and basicity density with the catalytic performance; TPO profiles of the used catalyst; the correlation between the amount of carbon deposits with the ratio of acidity/basicity; XRD and XPS of the used catalyst; and the regeneration performance of the used catalyst are provided. This material is available free of charge via the Internet at http://pubs.acs.org.

■ AUTHOR INFORMATION

Corresponding Author

*Tel.: +86-10-62772592. Fax: +86-10-62771149. E-mail: bqxu@mail.tsinghua.edu.cn.

Notes

The authors declare no competing financial interest.

■ ACKNOWLEDGMENTS

This work is partly supported by NSF of China (grant: 21033004).

■ REFERENCES

(1) Corma, A.; Iborra, S.; Velty, A. *Chem. Rev.* **2007**, *107*, 2441−2502.
(2) Chheda, J. N.; Huber, G. W.; Dumesic, J. A. *Angew. Chem., Int. Ed.* **2007**, *46*, 7164−7183.
(3) Datta, R.; Henry, M. *J. Chem. Technol. Biotechnol.* **2006**, *81*, 1119−1129.
(4) Fan, Y. X.; Zhou, C. H.; Zhu, X. H. *Catal. Rev.* **2009**, *51*, 293−324.
(5) Xu, Z.; Zhu, L.; Chen, H. In *Comprehensive Biotechnology*, 2nd ed.; Moo-Young, M., Butler, M., Webb, C., Moreira, A., Grodzinski, B., Cui, Z. F., Agathos, S., Eds; Elsevier: Amsterdam, 2011; Vol. 3, p 201−206.
(6) Lin, M. M. *Appl. Catal., A* **2001**, *207*, 1−16.
(7) Weissermel, K.; Arpe, H. J. In *Industrial Organic Chemistry*, 4th ed.; Wiley-VCH: Weinheim, Germany, 2003; Vol. *11*, p 291−296.
(8) Holmen, R. E. U.S. Patent 2,859,240, 1958.
(9) Sawicki, R. A. U.S. Patent 4,729,978, 1988.
(10) Paparizos, C.; Dolhyj, S. R.; Shaw, W. G. U.S. Patent 4,786,756, 1988.
(11) Zhang, J. F.; Lin, J. P.; Cen, P. L. *Can. J. Chem. Eng.* **2008**, *86*, 1047−1053.
(12) Hong, J. H.; Lee, J. M.; Kim, H.; Hwang, Y. K.; Chang, J. S.; Halligudi, S. B.; Han, Y. H. *Appl. Catal., A* **2011**, *396*, 194−200.
(13) Ghantani, V. C.; Lomate, S. T.; Dongare, M. K.; Umbarkar, S. B. *Green Chem.* **2013**, *15*, 1211−1217.
(14) Matsuura, Y.; Onda, A.; Ogo, S.; Yanagisawa, K. *Catal. Taday* **2014**, *226*, 192−197.
(15) Matsuura, Y.; Onda, A.; Yanagisawa, K. *Catal. Commun.* **2014**, *48*, 5−10.
(16) Blanco, E.; Delichere, P.; Millet, J. M. M.; Loridant, S. *Catal. Taday* **2014**, *226*, 185−191.
(17) Peng, J. S.; Li, X. L.; Tang, C. M.; Bai, W. *Green Chem.* **2014**, *16*, 108−111.
(18) Gunter, G. C.; Miller, D. J.; Jackson, J. E. *J. Catal.* **1994**, *148*, 252−260.
(19) Gunter, G. C.; Langford, R. H.; Jackson, J. E.; Miller, D. J. *Ind. Eng. Chem. Res.* **1995**, *34*, 974−980.
(20) Gunter, G. C.; Craciun, R.; Tam, M. S.; Jackson, J. E.; Miller, D. J. *J. Catal.* **1996**, *164*, 207−219.
(21) Wadley, D. C.; Tam, M. S.; Kokitkar, P. B.; Jackson, J. E.; Miller, D. J. *J. Catal.* **1997**, *165*, 162−171.
(22) Tam, M. S.; Gunter, G. C.; Craciun, R.; Miller, D. J.; Jackson, J. E. *Ind. Eng. Chem. Res.* **1997**, *36*, 3505−3512.
(23) Tam, M. S.; Craciun, R.; Miller, D. J.; Jackson, J. E. *Ind. Eng. Chem. Res.* **1998**, *37*, 2360−2366.

(24) Tam, M. S.; Jackson, J. E.; Miller, D. J. *Ind. Eng. Chem. Res.* **1999**, *38*, 3873−3877.
(25) Mok, W. S. L.; Antal, M. J.; Jones, M. *J. Org. Chem.* **1989**, *54*, 4596−4602.
(26) Wang, H. J.; Yu, D. H.; Sun, P.; Yan, J.; Wang, Y.; Huang, H. *Catal. Commun.* **2008**, *9*, 1799−1803.
(27) Sun, P.; Yu, D. H.; Fu, K. M.; Gu, M. Y.; Wang, Y.; Huang, H.; Ying, H. J. *Catal. Commun.* **2009**, *10*, 1345−1349.
(28) Sun, P.; Yu, D. H.; Tang, Z. C.; Li, H.; Huang, H. *Ind. Eng. Chem. Res.* **2010**, *49*, 9082−9087.
(29) Yan, J.; Yu, D. H.; Li, H.; Sun, P.; Huang, H. *J. Rare Earth* **2010**, *28*, 803−806.
(30) Yan, J.; Yu, D. H.; Sun, P.; Huang, H. *Chin. J. Catal.* **2011**, *32*, 405−411.
(31) Yu, D. H.; Sun, P.; Tang, Z. C.; Li, Z. X.; Huang, H. *Can. J. Chem. Eng.* **2011**, *89*, 484−490.
(32) Bett, J. A. S.; Christner, L. G.; Hall, W. K. *J. Am. Soc. Chem.* **1967**, *89*, 5535−5541.
(33) Bett, J. A. S.; Hall, W. K. *J. Catal.* **1968**, *10*, 105−113.
(34) Kibby, C. L.; Hall, W. K. *J. Catal.* **1973**, *29*, 144−159.
(35) Kibby, C. L.; Hall, W. K. *J. Catal.* **1973**, *31*, 65−73.
(36) Joris, S. J.; Amberg, C. H. *J. Phys. Chem.* **1971**, *75*, 3167−3171.
(37) Tsuchida, T.; Kubo, J.; Yoshioka, T.; Sakuma, S.; Takeguchi, T.; Ueda, W. *J. Catal.* **2008**, *259*, 183−189.
(38) Tsuchida, T.; Kubo, J.; Yoshioka, T.; Sakuma, S.; Takeguchi, T.; Ueda, W. J. *Jpn. Petrol. Inst.* **2009**, *52*, 51−59.
(39) Tao, L. Z.; Yan, B.; Liang, Y.; Xu, B. Q. *Green Chem.* **2013**, *15*, 696−705.
(40) Zheng, W. T.; Sun, K. Q.; Liu, H. M.; Xu, B. Q. *Int. J. Hydrogen Energy* **2012**, *37*, 11735−11747.
(41) Chai, S. H.; Wang, H. P.; Liang, Y.; Xu, B. Q. *Appl. Catal., A* **2009**, *353*, 213−222.
(42) Tao, L. Z.; Chai, S. H.; Zuo, Y.; Zheng, W. T.; Liang, Y.; Xu, B. Q. *Catal. Today* **2010**, *158*, 310−316.
(43) Elliott, J. C. In *Studies in Inorganic Chemistry*; Elsevier: Amsterdam, 1994; Vol. *18*, p 111−189.
(44) Ogo, S.; Onda, A.; Iwasa, Y.; Hara, K.; Fukuoka, A.; Yanagisawa, K. *J. Catal.* **2012**, *296*, 24−30.
(45) Winand, L.; Dallemagne, M. L.; Duyckaerts, G. *Nature* **1961**, *190*, 164−165.
(46) Winand, L.; Dallemagne, M. L. *Nature* **1962**, *193*, 369−370.
(47) Berry, E. E. *J. Inorg. Nucl. Chem.* **1967**, *29*, 317−327.
(48) Bonel, G.; Heughebaert, J. C.; Heughebaert, M.; Lacout, J. L.; Lebugle, A. *Ann. N.Y. Acad. Sci.* **1988**, *523*, 115−130.
(49) Sugiyama, S.; Miyamoto, T.; Hayashi, H.; Moffat, J. B. *J. Mol. Catal. A* **1998**, *135*, 199−208.
(50) Lu, H. B.; Camphell, C. T.; Graham, D. J.; Ratner, B. D. *Anal. Chem.* **2000**, *72*, 2886−2894.
(51) Kieswetter, K.; Bauer, T. W.; Brown, S. A.; Lente, F. V.; Merritt, K. *Biomaterials* **1994**, *15*, 183−188.
(52) El Shafei, G. M. S.; Philip, C. A.; Moussa, N. A. *J. Colloid Interface Sci.* **2004**, *277*, 410−416.
(53) Resende, N. S.; Nele, M.; Salim, V. M. M. *Thermochim. Acta* **2006**, *451*, 16−21.
(54) Lamonier, C.; Lamonier, J. F.; Aellach, B.; Ezzamarty, A.; Leglise, J. *Catal. Today* **2011**, *164*, 124−130.
(55) Krajewski, A.; Mazzocchi, M.; Buldini, P. L.; Ravaglioli, A.; Tinti, A.; Taddei, P.; Fagnano, C. *J. Mol. Struct.* **2005**, *744−747*, 221−228.
(56) Yasukawa, A.; Kandori, K.; Ishikawa, T. *Calcif. Tissue Int.* **2003**, *72*, 243−250.
(57) Aida, T. M.; Ikarashi, A.; Satio, Y.; Watanabe, M.; Smith, R. L., Jr.; Arai, K. *J. Supercrit. Fluids* **2009**, *50*, 257−264.
(58) Wojtczak, M.; Antczak, A.; Przybyt, M. *Food Addit. Contam., Part A* **2010**, *27*, 817−824.
(59) González, M. I.; Alvarez, S.; Riera, F. A.; Álvarez, R. *Desalination* **2008**, *228*, 84−96.
(60) West, R. M.; Braden, D. J.; Dumesic, J. A. *J. Catal.* **2009**, *262*, 134−143.
(61) Chai, S. H.; Tao, L. Z.; Yan, B.; Vedrine, J. C.; Xu, B. Q. *RSC Adv.* **2014**, *4*, 4619.
(62) Imizu, Y.; Kadoya, M.; Abe, H.; Itoh, H.; Tada, A. *Chem. Lett.* **1982**, *11*, 415−416.
(63) Onaka, M.; Ohta, A.; Sugatia, K.; Imizu, Y. *Appl. Catal., A* **1995**, *125*, 203−216.
(64) Tanabe, K.; Misono, M.; Ono, Y.; Hattori, H. In *Study in Surface Science and Catalysis*; Elsevier: Amsterdam, 1989; Vol. *51*, pp 260−261.
(65) Katryniok, B.; Paul, S.; Dumeignil, F. *Green Chem.* **2010**, *12*, 1910−1913.
(66) Guisnet, M. In Ertl, G.; H. Knözinger, Weitkamp, J. *Handbook of Heterogeneous Catalysis*; VCH: Weinheim, Germany, 1997; Vol. *2*, p 626.